

VideoFACT: Detecting Video Forgeries Using Attention, Scene Context, and Forensic Traces

Tai D. Nguyen^{*} Shengbang Fang Matthew C. Stamm
Drexel University

{tdn47, sf683, mcs382}@drexel.edu

Abstract

Fake videos represent an important misinformation threat. While existing forensic networks have demonstrated strong performance on image forgeries, recent results reported on the Adobe VideoSham dataset show that these networks fail to identify fake content in videos. In this paper, we propose a new network that is able to detect and localize a wide variety of video forgeries and manipulations. To overcome challenges that existing networks face when analyzing videos, our network utilizes both forensic embeddings to capture traces left by manipulation, context embeddings to exploit forensic traces' conditional dependencies upon local scene content, and spatial attention provided by a deep, transformer-based attention mechanism. We create several new video forgery datasets and use these, along with publicly available data, to experimentally evaluate our network's performance. These results show that our proposed network is able to identify a diverse set of video forgeries, including those not encountered during training. Furthermore, our results reinforce recent findings that image forensic networks largely fail to identify fake content in videos.

1. Introduction

Detecting fake and manipulated media is critical in the fight against misinformation. This has become an important challenge as recent advances in AI, such as deepfakes [16, 28, 60, 64, 75], generative adversarial networks (GANs) [1, 11, 19, 30–32, 65], and diffusion models [21, 33, 47, 54, 56, 57], have enabled the creation of visually realistic fake images and videos.

In response to this, significant research has been devoted to developing media forensic approaches capable of detecting image and video forgeries. These techniques operate by exploiting anomalous forensic traces left by manipulation or content falsification. Most existing forensics research has

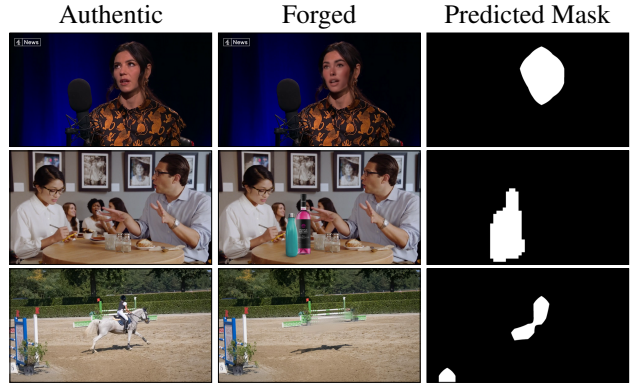


Figure 1. Sample video forgery localization results obtained using our proposed VideoFACT network on videos modified by deepfaking (Top), splicing in an object (Middle), and removing an object with inpainting (Bottom).

focused on detecting image forgeries. Several networks have achieved strong reported performance detecting and localizing fake content in images by directly learning to detect several known forgery types [2, 4, 7, 25, 39, 40, 67, 69, 72, 74], or by searching for localized anomalies in an image's forensic traces [10, 15, 27, 43, 66].

By contrast, comparatively little work has focused on video. Furthermore, the majority of existing video forensics research is devoted to detecting deepfakes. Several successful deepfake detection networks have been developed [20, 24, 26, 29, 37, 62, 68, 73]. However, many fake videos are not deepfakes and do not contain manipulated human faces. Deepfake detectors are unable to protect against these types of video forgeries.

Often, it is assumed that image forensic networks will perform well when used to individually analyze each frame in a video as if it were an image. Surprisingly, however, results presented in this paper as well as recent benchmarking results obtained by Adobe Research on its VideoSham dataset [45] show that these networks largely fail when applied to videos. As a result, there is a significant gap in the ability to detect a wide variety of fake videos.

In this paper, we propose a new network designed to detect a wide variety of video forgeries and manipulations. We name our network VideoFACT: Video Forensics using

^{*}Main author of this work

Attention, Context, and Traces. To overcome challenges that existing networks face when analyzing video, we observe that scene content has an important influence on the quality and quantity of local forensic information. Prior work has shown that some regions contain more forensic information of higher quality, while others contain little-to-no forensic information [13, 48, 58]. As a result, forensic traces have implicit dependencies on the scene content in the region from which they are extracted. Similarly, editing and falsification does not occur in random, independent spatial positions throughout a scene. Instead, a scene is typically modified to edit, add, or remove an object. As a result, in falsified content, forensic traces implicitly depends on spatial information.

VideoFACT is explicitly designed to exploit forensic traces’ contextual dependencies upon scene content as well as spatial dependencies. We accomplish this by producing both low-level forensic feature embeddings and low-level context embeddings for each local analysis region. These context embeddings provide information that accounts for variations in the forensic embeddings due to scene content. We leverage both embeddings by using a deep, transformer-based attention module to provide spatial attention information to two different subnetworks that perform frame-level forgery detection and pixel-level forgery localization.

This deep attention mechanism provides our network with multiple benefits. It enables our network to attend to regions with high-quality forensic information while de-emphasizing regions with lower-quality information that may cause false alarms. It is also able to learn and exploit complex relationships between the forensic embeddings, context embeddings, and spatial position to better identify fake content. We note that recent work has begun to utilize shallow attention mechanisms in forensic networks [10, 66]. However, as our results in Section 5 show, these shallow mechanisms are unable to produce strong results on video forgeries. By contrast, our deep transformer-based attention mechanism is able to overcome challenges encountered by prior work and produce strong video forgery detection and localization results.

The main contributions of this work are as follows: (1) We propose a new network capable of detecting a wide many types of manipulations and fake content in video. (2) We utilize the novel concept of context embeddings to account for natural variations in forensic traces due to scene content. (3) We utilize spatial attention, produced by a deep transformer-based attention module, that enables our network to rely more heavily on scene regions with high-quality forensic information while de-emphasizing others with poor information. (4) We develop multiple new datasets for training and benchmarking video forensic algorithms. Currently, there are no video forgery datasets made for network training and only the VideoSham dataset for video forgery detection benchmarking. Our new datasets are composed not only of standard video manipulations such as splicing, but also ad-

vanced AI-based content manipulation techniques. (5) We provide experimental evidence that existing forensic networks designed on images largely fail when used to analyze videos forgeries. (6) We experimentally demonstrate that our proposed network can detect a wide variety of video forgery and manipulation types.

2. Related Work

Most previous work on forgery detection and localization focuses on images. The earliest work on this topic developed hand-designed detectors for specific types of image manipulation detection [17, 34, 35, 49, 51, 53, 59]. Following the rise of deep learning, researchers developed a wide variety of new forensic networks capable of simultaneously identifying a broad range of editing operations [2, 4, 7, 25, 39, 40, 67, 69, 72, 74]. These algorithms achieve strong performance detecting manipulations that they are trained on, but typically encounter difficulties when confronted with new manipulations outside of the training set. Similar approaches have been developed to detect synthetic image, following the rise of GANs capable of creating realistic fake human faces and objects [8, 38, 63, 70].

Most real world manipulated images are made using a combination of multiple editing operations that are unknown to the forensic algorithms at the time of analysis. To address this, researchers have developed approaches that extract local forensic features throughout an image, then search for anomalous traces [10, 15, 27, 43, 66, 71]. These algorithms have achieved strong performance detecting and localizing fake content in images. Little work has been done to develop similar approaches explicitly for video. There is a rapidly growing body of research devoted to detecting deepfake videos [20, 24, 26, 29, 37, 62, 68, 73]. While these networks are able to successfully detect deepfakes, they cannot be used to detect other video forgeries because they explicitly or implicitly exploit physiological models of the human face or head. Other work has focused on detecting temporal video manipulations, as opposed to content falsification [18, 22].

3. Proposed Approach

An overview of VideoFACT can be seen in Figure 2. Our network first divides a frame into non-overlapping analysis blocks of size 128×128 pixels. Next, each block is sent to two parallel low-level feature extractors: one designed to produce forensic feature embeddings f and another that produces context embedding c that captures relevant local information about the scene. A joint set of low-level feature embeddings x , which is produced by concatenating the forensic and context embeddings, is passed to a transformer-based attention module, which produces a series of L different spatial attention maps m_ℓ . These attention maps are then used to weight the joint feature embeddings by spatial at-

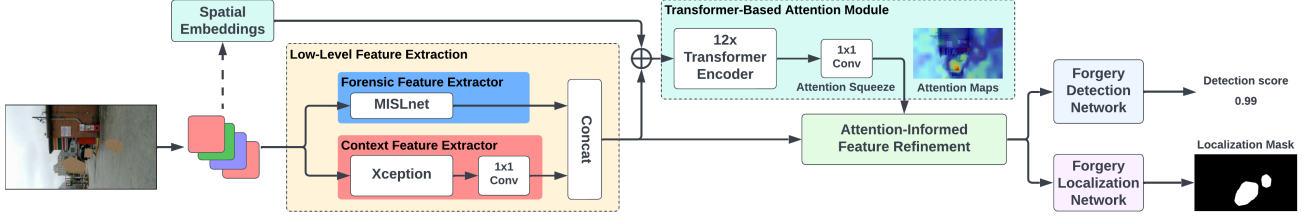


Figure 2. Overview of our proposed VideoFACT network for video forgery detection and localization. Our network extracts both forensic feature embeddings and scene context embeddings from local analysis blocks. These embeddings are concatenated, then weighted by attention maps produced by a transformer-based attention module. The attention scaled joint feature embeddings are passed to two different subnetworks that produce frame-level detection decisions and pixel-level forgery masks.

tention. The resulting attention weighted embeddings y are then used by two parallel subnetworks, which independently perform frame-level forgery detection and pixel-level forgery localization.

3.1. Low-Level Feature Extraction

VideoFACT’s network architecture consists of two low-level feature extractors working in tandem: the Forensic Feature Extractor (FFE) and the Contextual Feature Extractor (CFE). Each analysis block b_k is independently passed through each extractor to produce a forensic feature embedding f_k and a context feature embedding c_k .

Forensic Feature Embeddings. We use a CNN $g(\cdot)$ to produce dedicated forensic feature embeddings for each block. To produce these embeddings, g is pre-trained to discriminate between the source camera model used to capture each block in a separate training set. This is inspired by an approach widely taken in image forensics, where a CNN trained to discriminate between source camera models is utilized to learn generic forensic feature embeddings [14, 15, 27, 41, 43, 44]. These embeddings have been shown to capture both forensic information about the source and manipulation or processing history of a block.

We implement g using a MISLnet [5] backbone. This network was chosen because it is both lightweight and has been demonstrated to achieve strong performance on several forensic tasks in prior research [6, 9, 42–44]. The loss used during the pre-training phase of g is defined as:

$$\mathcal{L}_F = - \sum_{\ell=1}^n t_{\ell} \cdot \log(g(d_k))_{\ell} \quad (1)$$

where n is the number of different camera models classes, $t_{\ell} = 1$ if the block d_k was captured by the ℓ^{th} camera model and 0 otherwise. After pre-training, the softmax layer is discarded. This network is not updated during the initial training phase but is allowed to evolve slowly during subsequent fine-tuning phases.

Context Feature Embeddings. The context feature extractor $h(\cdot)$ produces embeddings c that provide information about a scene that contextualizes the forensic embeddings. Prior research has shown that scene content can have important effects on forensic features. Specifically, the amount and quality of forensic information in an analysis window depends on the local illumination, texture, compression pa-

rameters, and several other factors [13, 48, 58]. By jointly analyzing forensic and context feature embeddings, later portions of our network can adjust how they interpret forensic features in a particular block to make better forensic decisions. We implement h by using an Xception [12] network backbone that is modified to use only a single middle flow module, followed by a 1×1 layer to reduce the feature embedding dimension.

Joint Feature Extraction. After obtaining both forensic and context embeddings for each block, we produce the joint feature embeddings x by concatenating f and c , i.e.,

$$x_k = \text{Concat}(f_k, c_k) \quad (2)$$

This process is repeated for every analysis block in the video frame to produce N arrays of joint feature embedding. Each embedding is 768 elements long.

3.2. Transformer-Based Attention Module

The sequence of joint embeddings is passed to the transformer-based attention module, which is designed to produce a series of L different spatial attention maps. To encode spatial position information, a vector of 1-D learnable spatial embeddings is added to the joint embeddings before being passed to the transformer. The transformer consists of twelve transformer encoder blocks stacked on top of one another. The output of the transformer is passed to an “Attention Squeeze” layer that consists of L , 1×1 convolutional kernels. This “squeezes” down the high dimensional output to a series of L different $M \times N$ spatial attention maps m_l . Each entry of the L attention maps m_l corresponds to the network’s attention score for the corresponding joint feature embedding at that position.

Fig. 3 shows an example of a spatial attention map produced by our transformer-based attention module, as well as the corresponding the unaltered video frame. From this example, we can see that VideoFACT attends to regions that contain high-quality forensic traces, i.e. regions with sufficient texture, illumination, etc. By contrast, regions known to contain low-quality forensic information such as the sky are de-emphasized. Often, these regions will cause false alarms because their low-quality forensic traces will appear anomalous with respect to the rest of the traces throughout the scene. By not attending to these regions, our network can avoid these false alarms.

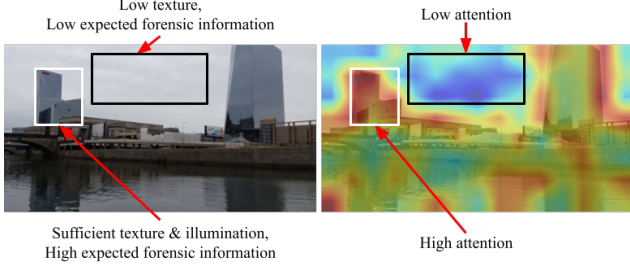


Figure 3. Example showing the effect of our attention module. The attention map produced for this frame gives large weights (shown in red) to regions with high quality forensic information - i.e. it has sufficient texture, illumination, no blurring, etc. Regions with low quality forensic information are given low weight (shown in blue).

3.3. Attention-Informed Feature Refinement

After the transformer-based module produces a set of L attention maps, these maps are used to weight the low-level joint feature embeddings by spatial attention. The joint feature embedding x_k at the k^{th} spatial location is weighted by the corresponding k^{th} entry in the l^{th} attention map. This enables the network to attend to feature embeddings at spatial locations with higher amounts of higher-quality forensic information. This process is repeated for all L spatial attention maps. Then the resulting features are summed to produce the attention-informed features y , such that:

$$y_k = \sum_{\ell=1}^L x_k m_{k,\ell} \quad (3)$$

3.4. Detection and Localization

VideoFACT produces two outputs: a frame-level detection score and a pixel-level localization mask. The localization mask is disregarded if the detection score indicates no forged content exists. Our network separately analyzes the attention-informed feature embeddings using two different subnetworks for localization and detection.

Detection Network. The detection network $p(\cdot)$ consists of two 1×1 Conv + ReLU layers for dimension reduction with 200, and 2 kernels, respectively, followed by a fully connected and a softmax layer to output two neurons, one corresponds to pristine and the other corresponds to being falsified. The detection loss for this subnetwork is the cross-entropy loss between the label and the predicted output:

$$\mathcal{L}_D = - \sum_{n=1}^2 w_n \log(p_n) \quad (4)$$

where p_n is the output of $p(\cdot)$ and the w_n is the one-hot vector indicate whether the video is manipulated.

Localization Network. The localization network $q(\cdot)$ is composed of four 1×1 Convolutional layers with 192, 96, 12, and 1 kernel, respectively. We use ReLU activation except in the last layer, which uses sigmoid activation to output the block-wise probability of being manipulated.

The localization loss is built on top of this subnetwork. We define the localization loss to be the sum of block-wise

cross-entropy loss. Which is:

$$\mathcal{L}_L = \sum_{k=1}^N -z_k \log(q_k) + (1 - z_k) \log(1 - q_k) \quad (5)$$

where q_k is the prediction of $q(\cdot)$ for the corresponding block b_k , and z_k is the true probability of the block being manipulated. Because a block could contain a partial of manipulated region, we define z_k as the ratio of manipulated pixels in the ground-truth mask:

$$z_k = \sum_{i,j \in \mathbb{P}_k} M_{i,j} / |\mathbb{P}_k| \quad (6)$$

where \mathbb{P}_k is the set of pixel coordinates that belong to block k , and M is the ground-truth binary mask.

During inference, we achieve the pixel-level predicted mask from the block-wise prediction. We first threshold the block-level prediction probabilities. Typically, there are two peaks in this histogram of block-level probabilities, one due to unaltered blocks and the other due to manipulated blocks. The threshold is chosen as the location of the first minima to the right of the first histogram peak (i.e. the one induced by unaltered blocks). After thresholding, we use the flood-fill morphological algorithm to remove holes from the localization mask. A final pixel-level mask is produced by scaling the block-level mask to the full video frame size using bilinear interpolation.

Joint Training. To train the entire network, we define the total loss as a linear combination of the detection and localization losses:

$$\mathcal{L} = \alpha \mathcal{L}_D + (1 - \alpha) \mathcal{L}_L \quad (7)$$

where $\alpha \in (0, 1)$ is the weight to balance the frame-level detection loss and the block-level localization loss.

3.5. Multi-Stage Training Protocol

Our network training protocol consists of five stages. In the first three stages, the training datasets consist of videos falsified with manipulations that are successively more difficult to detect. This enables the network to progressively learn better features by refining those learned in the previous stage. In Stage 1, we use the Video Camera Model Splicing dataset (VCMS), which contains spliced content from other videos. Because splicing induces source camera inconsistencies within a frame, the forensic embeddings learned by the FFE in the pre-training phase are well suited to identify these manipulations. In Stages 2 and 3, we train the network with the Video Perceptually Visible Manipulation dataset (VPVM) and Video Perceptually Invisible Manipulation datasets (VPIM), respectively. These datasets, which are described in Section 4, contain videos manipulated using standard editing operations applied with different strengths.

In the last two stages, we improve the generalizability of our network by training on multiple datasets with varying manipulations and scene content. In Stage 4, we fine-tune the network using all three previous datasets simultaneously (VCMS, VPVM and VPIM). In Stage 5, we further fine-tune

the model by incorporating three auxiliary datasets made from images in the Camera Model Identification Database (CMID) first used in [5, 6]. We create these auxiliary training datasets from the CMID, because it captures scenes with different content and distribution than the Video-ACID dataset. This increases the diversity of data on which our network is trained. These auxiliary datasets are made using the same process used to create the three video datasets, resulting in one dataset with spliced content (ICMS), one with perceptually visible manipulations (IPVM), and one with perceptually invisible manipulations (IPIM).

4. Video Forgery Datasets

Currently, there are no publicly available datasets of manipulated video large enough to train forgery detection and localization networks. Similarly, there are almost no datasets suitable to evaluate such networks, with the notable exception of the Adobe VideoSham dataset, which was released in July 2022 [46]. To address this issue, we created a series of new video manipulation datasets for training and evaluating our network. These are divided into two subsets. Set A contains videos modified using standard manipulations, e.g. splicing and local editing, etc. Set B contains “in-the-wild” videos made using more sophisticated editing operations such as inpainting, deepfakes, etc. All datasets will be made publicly available upon publication of this paper.

4.1. Set A: Standard Video Manipulations Datasets

We made three datasets by applying different sets of standard manipulations to videos from the Video-ACID [23] dataset. All three datasets were made using a common procedure. First, we created binary ground-truth masks specifying the tamper regions for each video. These tamper regions correspond to multiple randomly chosen shapes with random sizes, orientations, and placements within a frame. Fake videos were created by choosing a mask, then manipulating content within the tamper region. Pristine copies of each original video were also retained to create a set of authentic videos. All video frames (both manipulated and authentic) were re-encoded as H.264 videos using FFmpeg [61] with a constant rate factor of 23 and a 30 FPS frame rate.

Each dataset in Set A corresponds to a different manipulation type. The **Video Camera Model Splicing (VCMS)** dataset contains videos with content spliced in from other videos. The **Video Perceptually Visible Manipulation (VPVM)** dataset contains content modified using common editing operations such as contrast enhancement, smoothing, sharpening, blurring, etc. applied with strengths that can be visually detected. The **Video Perceptually Invisible Manipulation (VPIM)** dataset was made in a similar fashion to the VPVM, but using much smaller manipulation strengths to create challenging forgeries. For each dataset, we made 3200 videos (96000 frames) for training, 520 videos (15600

Stage	Dataset	Optimizer	Epochs	Initial Lr	Decay rate	Decay step
1	A	SGD	6	$1.0e-4$	0.75	2
2	B	SGD	6	$8.5e-5$	0.85	2
3	C	SGD	23	$8.5e-5$	0.85	2
4	A, B, C	SGD	10	$8.5e-5$	0.85	2
5	A, B, C, D, E, F	SGD	9	$5.0e-5$	0.85	2

Table 1. Training parameters for different training stages of our model. We denote: A=VCMS, B=VPVM, C=VPIM, D=ICMS, E=IPVM, F=IPIM.

frames) for validation, and 280 videos (8400 frames) for testing.

4.2. Set B: In-the-Wild Manipulated Datasets

We used three “in-the-wild” datasets to evaluate our network: VideoSham [46] created by Adobe Research, and both the Inpainted Video and Deepfake Video datasets created by us. These datasets contain advanced, challenging manipulations applied to videos with scene content that significantly differs from our training datasets.

VideoSham [46] contains high-quality videos manipulated by professional editors using multiple techniques. Because this work focuses exclusively on identifying fake content, we excluded videos with audio track or temporal manipulations. Additionally, videos of with resolution less than our network’s input size of 1920×1080 pixels were also excluded. This resulted in 7897 frames from 32 manipulated videos, and 12746 frames from 64 authentic videos.

Our **Inpainted Video** dataset was made by using inpainting to remove objects specified by segmentation masks from videos in the Densely Annotated Video Segmentation (DAVIS) dataset [50]. Inpainting was performed with E2FGVI-HQ [36] using the authors’ recommended settings, producing output videos in 540p resolution. They were then resized to 1080p so that they could be analyzed by our network. This dataset contains both authentic and manipulated subsets that each contain of 9312 frames from 90 videos.

Our **Deepfake Video** dataset was made by creating deepfakes from a set of publicly available videos of celebrities downloaded from YouTube. These deepfakes were generated using DeepFaceLab [16] to ensure that all fake videos were of 1080p resolution, created as a video rather than a sequence of individually compressed images, and utilized deepfake creation software that is currently most commonly used in the wild. Our dataset consists of a manipulated subset of 300 frames from 10 high-quality deepfake videos and an unaltered subset of 300 frames from 10 original videos. We note that this dataset was created to evaluate and demonstrate our network’s ability to detect a wide variety of video forgeries. Our purpose is not to create a dedicated deepfake detector.

5. Experiments

Training Implementation. We implemented our network using PyTorch and trained it using an NVIDIA RTX 3090. The network input size is 1080×1920 pixels (a single

Method	VCMS				VPVM				VPIM			
	Det. mAP	Det. ACC	Loc. MCC	Loc. F1	Det. mAP	Det. ACC	Loc. MCC	Loc. F1	Det. mAP	Det. ACC	Loc. MCC	Loc. F1
FSG [43]	0.445	0.497	0.001	0.064	0.431	0.480	0.004	0.067	0.485	0.494	0.011	0.065
EXIFnet [27]	0.610	0.502	0.208	0.230	0.568	0.501	0.213	0.236	0.509	0.500	0.026	0.124
Noiseprint [15]	0.521	0.500	0.041	0.030	0.495	0.500	0.012	0.013	0.511	0.500	0.010	0.010
ManTra-Net [66]	0.451	0.500	0.079	0.114	0.526	0.500	0.110	0.145	0.513	0.500	0.025	0.064
MVSS-Net [10]	0.883	0.602	0.545	0.557	0.644	0.529	0.267	0.279	0.482	0.492	0.018	0.042
Ours	0.995	0.987	0.530	0.526	0.980	0.950	0.676	0.697	0.869	0.797	0.515	0.547

Table 2. Frame-level detection and pixel-level localization performance on Set A Standard Video Manipulations datasets - VCMS, VPVM, VPIM.

Method	Deepfake Video				Inpainted Video				VideoSham			
	Det. mAP	Det. ACC	Loc. MCC	Loc. F1	Det. mAP	Det. ACC	Loc. MCC	Loc. F1	Det. mAP	Det. ACC	Loc. MCC	Loc. F1
FSG [43]	0.450	0.515	0.204	0.137	0.386	0.452	0.208	0.302	0.596	0.538	0.162	0.246
EXIFnet [27]	0.447	0.492	0.180	0.133	0.635	0.501	0.160	0.244	0.584	0.555	0.148	0.246
Noiseprint [15]	0.591	0.500	0.010	0.062	0.601	0.500	0.091	0.232	0.422	0.447	0.034	0.206
ManTra-Net [66]	0.450	0.500	0.004	0.042	0.499	0.500	0.009	0.055	0.551	0.553	0.009	0.058
MVSS-Net [10]	0.464	0.498	0.199	0.189	0.341	0.435	0.058	0.227	0.595	0.449	0.142	0.096
Ours	0.666	0.648	0.415	0.410	0.782	0.687	0.225	0.309	0.691	0.656	0.193	0.312

Table 3. Frame-level detection and pixel-level localization performance on Set B’s “in-the-wild” datasets - Deepfake Video, Inpainted Video, VideoSham [45]

1080p frame). We first pre-trained the FFE on the Video-ACID dataset using the Stochastic Gradient Descent (SGD) optimizer with an initial learning rate of $1.0e-3$, momentum of 0.95, and an exponential decay-rate of 0.5 for every 2 epochs. After pretraining the FFE, we trained the entire network following the five stages described in Section 3.5 with different training parameters shown in Table 1. Throughout the stages, we set $\alpha = 0.4$.

Evaluation Datasets. We evaluated the frame-level performance of our proposed network and competing networks on the six datasets described in Section 4.

Evaluation Metrics. For frame-level manipulation detection, we report the mean average precision (mAP) for each dataset. Also, we provide the average accuracy (ACC) per datasets using a unified threshold of 0.5 to reflect real-world’s performance. For forgery localization (i.e. pixel-level manipulation detection) we use F1 and MCC scores to evaluate the correlation between the ground-truth and predicted masks, which are binarized with a threshold of 0.5.

5.1. Detection and Localization Performance

We compared the performance of VideoFACT to several existing image forensic networks including Forensic Similarity Graphs (FSG) [43], EXIFnet [27], Noiseprint [15], ManTra-Net [66], and MVSS-Net [10], representing a broad spectrum of successful techniques for performing forgery detection and localization in images. We note that Noiseprint and Mantra-Net do not automatically perform detection. To fairly compare against these networks, we obtain frame-level detection scores by computing the average normalized per-pixel detection probability.

Set A: Standard Video Manipulations. Table 2 shows the performance of our proposed network and competing networks on the three Standard Video Manipulations datasets in Set A. These results show that VideoFACT achieves the best performance by a large margin on these datasets. The only exception is for the VCMS dataset, where MVSS-Net’s localization performance is slightly better than ours, though

still comparable. Except for this case, existing networks largely do no better than a random guess (i.e. $mAP = 0.5$ and $MCC = 0$). This phenomenon can be clearly seen in both Table 2 and the qualitative results presented in Fig 4. These results reinforce similar findings reported in the VideoSham paper [46], that is, existing networks are unable to adapt to forensic differences between image and video forgeries.

Set B: “In-the-Wild” Datasets. Table 3 shows the performance of our network and existing networks on the three “in-the-wild” datasets, which consists much more complex and challenging forgeries. These results show that VideoFACT uniformly achieves the best detection and localization performance over all three datasets. By contrast, existing approaches typically fail on these challenging datasets. This can be observed in the qualitative results presented in Fig. 4. These results further solidify our observations on Set A and results reported in the VideoSham paper [45] that existing image forensic networks largely fail on falsified videos.

For the Deepfake Video dataset, we note that while our network significantly outperforms image forensic networks, it is unlikely to outperform dedicated deepfake detectors [26, 29, 37, 73]. This is because our network doesn’t leverage useful semantic information such human face models that deepfake detectors typically do. Despite this, these results show that our network can still achieve reasonable performance without explicitly training on deepfakes.

Additionally, we note that videos in the Inpainted Video dataset have been resized up to 1080p resolution. This is important because it is well-known that rescaling significantly downgrades the quality of forensic information. Despite this, we can still achieve good detection and localization performance on this dataset.

The results we obtain on the VideoSham dataset are influenced by the size of the falsified region in each video. Some of these videos contain fake content that is much smaller than the size of our network’s 128×128 analysis windows. Our network has a difficult time identifying these forgeries. Despite this, we still achieve better performance than other



Figure 4. This figure shows localization results from our proposed network as well as FSG [43], EXIFnet [27], Noiseprint [15], ManTra-Net [66], and MVSS-Net [10] on six different datasets, VCMS, VPVM, VPIM, Deepfake Video, Inpainted Video and VideoSham [45]. Our proposed network correctly identifies the manipulated area in videos falsified using a wide variety of forgery operations.

existing image forensic networks on this dataset.

5.2. Discussion

From the results presented in Tables 2 and 3, we can see that existing approaches, which reported strong performance on image forgeries, largely fail on video. There are multiple reasons why this may occur.

Effects of Video Compression. Coding and compression is well-known to have a significant effect on forensic traces [3, 35, 52]. One key reason why existing networks suffer significant performance decreases on video is likely due to differences between image and video compression.

Existing forgery detection networks are trained and validated using images. While many of these networks are resilient to JPEG effects, it is important to note that JPEG operates in the same manner throughout an image, irrespective of the underlying scene content. As a result, JPEG has a uniform effect on the forensic traces throughout an image.

By contrast, video compression does not operate in a spatially uniform manner. Modern standards like H.264 utilize a large number of macroblock types within a single frame, which are chosen based on the underlying scene content, motion, and several other factors [55]. Different macroblock types employ different coding techniques and parameters, resulting in different regional compression strengths throughout a frame. This can induce localized inconsistencies in

forensic traces, which will cause existing networks to incorrectly flag some regions as fake or manipulated.

False Alarm Effects. Another important reason why our network outperforms existing networks is its ability to avoid certain types of false alarms in unmanipulated regions. An example of this can be seen in Fig. 5. Here, existing networks produce false alarms in different ways that can be grouped according to how each network operates.

One set of existing approaches, such as EXIFnet, FSG, and Noiseprint, identify fake content by searching for anomalous forensic traces. These networks will produce false alarms in scene regions that contain little forensic information such as the sky. This is because these networks will often mistake low quality forensic traces for anomalous traces.

Another set of approaches, such as ManTra-Net and MVSS-Net, seek to learn good forgery detection features by analyzing noise residuals and edge information. These techniques can false alarm when highly salient foreground objects naturally exhibit different statistics from background objects. This effect occurs in the man sitting on the rock in Fig. 5. This natural variation will cause the noise residuals and edge information in the foreground objects to appear anomalous to these networks.

How Our Network Overcomes These Effects. Our network’s use of context embeddings and spatial attention enables it to be much more resilient to the effects described

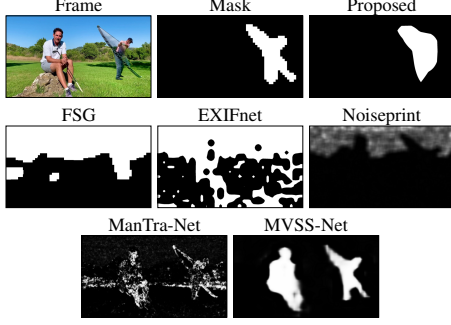


Figure 5. Example showing scene conditions that typically cause competing approaches to false alarm. Systems like FSG, EXIFnet, and Noiseprint will mistake traces in smooth regions such as the sky for anomalous traces due to editing. Networks like ManTra-Net and MVSS-Net mistake naturally occurring differences in noise statistics between foreground and background objects as caused by editing. Our network is able to use scene context and attention to control for these effects.

above. Our deep attention module allows our network to learn which scene regions contain high quality forensic information. Therefore, VideoFACT relies more heavily on these regions when making decisions and avoid many of the false alarm issues faced by other networks. Additionally, local context information enables our network to control for local variations in forensic traces induced by video compression as well as naturally occurring statistical variations induced by scene content.

Failure Cases and Limitations. We identified several common failure cases experienced by our network by examining videos in the “in-the-wild” datasets. Specifically, our network often miss-detects when: (1) The falsified region is very small, in particular when its area is much smaller than our 128×128 pixels analysis window. (2) Both the manipulated region and background have similar poor lighting conditions, and (3) The manipulated region has been altered by color swaps. Additionally, our network has limitations including: (1) It doesn’t exploit temporal effects or correlations between frames. (2) Our current implementation is only suitable for a fixed input video resolution of 1080p.

6. Ablation Study

We conducted multiple ablation experiments to validate the importance of various components in VideoFACT’s architecture. We trained each of the network variants using the same settings as the proposed method and assessed their performance on VideoSham. A summary of our experiments is shown in Table 4.

Influence of FFE. Removing FFE, we see the detection mAP drops from 0.691 to 0.646 and localization F1 from 0.258 to 0.209. This shows that the FFE is necessary to boost both performance and generalizability.

Influence of CFE. Without the CFE, every metric has a significant reduction. This shows that contextual information is crucial in the network getting a more comprehensive picture of the video forensic information.

Influence of the Transformer-Based Attention Mod-

Setup	Component					VideoSham			
	FFE	CFE	Trans-former	Attn. maps	Data comb.	Det. ACC	Det. mAP	Loc. F1	Loc. MCC
Proposed	+	+	+	3	Add	0.656	0.691	0.258	0.168
No FFE	—	+	+	3	Add	0.610	0.646	0.209	0.118
No CFE	+	—	+	3	Add	0.586	0.635	0.163	0.043
No Transformer Module	+	+	—	—	—	0.601	0.626	0.144	0.000
No Transformer	+	+	—	3	Add	0.533	0.538	0.140	0.048
No Attention Squeeze	+	+	+	—	—	0.622	0.656	0.254	0.120
1 Attention Map	+	+	+	1	Add	0.610	0.655	0.175	0.121
10 Attention Maps	+	+	+	10	Add	0.622	0.676	0.212	0.127
Diff. Feat. Refine	+	+	+	3	Concat	0.614	0.684	0.162	0.091

Table 4. Ablation study of the components in our proposed network and their performance evaluations.

ule. In this model variant, we removed the entire Transformer-Based Attention Module. The joint embeddings were fed directly into the detector and the localizer networks. This variant resulted in a substantial performance drop across the board. The detection metrics suggest that this network only does slightly better than random guess. Therefore, this module is a critical part of VideoFACT.

Influence of the Transformer. We measure the importance of the Transformer itself by replacing it with six fully connected layers with ReLU as the activation function. In this scenario, the model performs at a level close to random guess. Therefore, this cements the necessity of the Transformer for our network.

Influence of the Attention Squeeze. In this scenario, we connect the output of the Transformer directly to the detector and localizer, bypassing the Attention Squeeze component. From Table 4, we see that this variant underperforms in both detection and localization. Hence, the Attention Squeeze component is essential in boosting the model’s generalizability. We also try using 1, 3 (proposed) and 10 attention maps. Results show that using 3 attention maps yields the best performance.

Influence of different Feature Refinement approaches. Instead of the proposed approach, we concatenate all three sets of weighted spatially contextualized forensic embeddings. Results show that both detection and localization performance drop significantly. Therefore, the proposed method is the optimal choice.

7. Conclusion

In this paper, we propose a new network, VideoFACT, to detect and localize a broad range of video forgeries and manipulations. Our network does this by utilizing both forensic embeddings to capture traces left by manipulation, context embeddings to exploit forensic traces’ conditional dependencies upon scene content, and spatial attention provided by a deep, transformer-based attention mechanism. We create several new video forgery datasets, which we used along with the Adobe VideoSham dataset to experimentally evaluate our network’s performance. Our results show that our proposed network is able to identify a diverse set of video forgeries, including those not encountered during training.

Furthermore, our results show that existing image forensic networks largely fail to identify fake content in video.

References

- [1] Rameen Abdal, Peihao Zhu, Niloy J. Mitra, and Peter Wonka. Styleflow: Attribute-conditioned exploration of stylegan-generated images using conditional continuous normalizing flows. *ACM Trans. Graph.*, 40(3), may 2021. **1**
- [2] Jawadul H. Bappy, Amit K. Roy-Chowdhury, Jason Bunk, Lakshmanan Nataraj, and B. S. Manjunath. Exploiting spatial structure for localizing manipulated image regions. In *Proceedings of the IEEE International Conference on Computer Vision (ICCV)*, Oct 2017. **1, 2**
- [3] Belhassen Bayar and Matthew C. Stamm. On the robustness of constrained convolutional neural networks to jpeg post-compression for image resampling detection. In *ICASSP*, pages 2152–2156, 2017. **7**
- [4] Belhassen Bayar and Matthew C. Stamm. Constrained convolutional neural networks: A new approach towards general purpose image manipulation detection. *IEEE Trans. Inform. Forensics and Security*, 13(11):2691–2706, 2018. **1, 2**
- [5] Belhassen Bayar and Matthew C. Stamm. Constrained convolutional neural networks: A new approach towards general purpose image manipulation detection. *IEEE Trans. Inform. Forensics and Security*, 13(11):2691–2706, 2018. **3, 5**
- [6] Belhassen Bayar and Matthew C. Stamm. Towards open set camera model identification using a deep learning framework. In *ICASSP*, pages 2007–2011, 2018. **3, 5**
- [7] Jason Bunk, Jawadul H. Bappy, Tajuddin Manhar Mohammed, Lakshmanan Nataraj, Arjuna Flenner, B.S. Manjunath, Shivkumar Chandrasekaran, Amit K. Roy-Chowdhury, and Lawrence Peterson. Detection and localization of image forgeries using resampling features and deep learning. In *CVPRW*, pages 1881–1889, 2017. **1, 2**
- [8] Keshigeyan Chandrasegaran, Ngoc-Trung Tran, Alexander Binder, and Ngai-Man Cheung. Discovering transferable forensic features for cnn-generated images detection. In *ECCV*, pages 671–689, Cham, 2022. Springer Nature Switzerland. **2**
- [9] Chen Chen, Xinwei Zhao, and Matthew C. Stamm. Mislgan: An anti-forensic camera model falsification framework using a generative adversarial network. In *IEEE Intl. Conf. Image Processing*, pages 535–539, 2018. **3**
- [10] Xinru Chen, Chengbo Dong, Jiaqi Ji, Juan Cao, and Xirong Li. Image manipulation detection by multi-view multi-scale supervision. In *ICCV*, pages 14185–14193, October 2021. **1, 2, 6, 7**
- [11] Yunje Choi, Minje Choi, Munyoung Kim, Jung-Woo Ha, Sunghun Kim, and Jaegul Choo. Stargan: Unified generative adversarial networks for multi-domain image-to-image translation. In *CVPR*, June 2018. **1**
- [12] Francois Chollet. Xception: Deep learning with depthwise separable convolutions. In *CVPR*, July 2017. **3**
- [13] Xiaoyu Chu, Yan Chen, Matthew C Stamm, and KJ Ray Liu. Information theoretical limit of media forensics: The forensicability. *IEEE Transactions on Information Forensics and Security*, 11(4):774–788, 2015. **2, 3**
- [14] Davide Cozzolino, Giovanni Poggi, and Luisa Verdoliva. Splicebuster: A new blind image splicing detector. In *2015 IEEE International Workshop on Information Forensics and Security (WIFS)*, pages 1–6, 2015. **3**
- [15] Davide Cozzolino and Luisa Verdoliva. Noiseprint: A cnn-based camera model fingerprint. *IEEE Trans. Inform. Forensics and Security*, 15:144–159, 2020. **1, 2, 3, 6, 7**
- [16] Ivan Perov et. al. Deepfacelab: A simple, flexible and extensible face swapping framework. *CoRR*, abs/2005.05535, 2020. **1, 5, 13**
- [17] Jessica Fridrich and Jan Kodovsky. Rich models for steganalysis of digital images. *IEEE Trans. Inform. Forensics and Security*, 7(3):868–882, 2012. **2**
- [18] Edgar González Fernández, Ana Lucila Sandoval Orozco, and Luis Javier García Villalba. Digital video manipulation detection technique based on compression algorithms. *IEEE Transactions on Intelligent Transportation Systems*, 23(3):2596–2605, 2022. **2**
- [19] Ian Goodfellow, Jean Pouget-Abadie, Mehdi Mirza, Bing Xu, David Warde-Farley, Sherjil Ozair, Aaron Courville, and Yoshua Bengio. Generative adversarial networks. *Commun. ACM*, 63(11):139–144, oct 2020. **1**
- [20] David Güera and Edward J. Delp. Deepfake video detection using recurrent neural networks. In *IEEE Intl. Conf. Adv. Video and Signal Based Surveillance*, pages 1–6, 2018. **1, 2**
- [21] Jonathan Ho, Chitwan Saharia, William Chan, David J Fleet, Mohammad Norouzi, and Tim Salimans. Cascaded diffusion models for high fidelity image generation. *J. Mach. Learn. Res.*, 23:47–1, 2022. **1**
- [22] B. Hosler, O. Mayer, B. Bayar, X. Zhao, C. Chen, J. A. Shackelford, and M. C. Stamm. A video camera model identification system using deep learning and fusion. In *ICASSP*, pages 8271–8275, 2019. **2**
- [23] Brian C Hosler, Xinwei Zhao, Owen Mayer, Chen Chen, James A Shackelford, and Matthew C Stamm. The video authentication and camera identification database: A new database for video forensics. *IEEE Access*, 7:76937–76948, 2019. **5**
- [24] Chih-Chung Hsu, Yi-Xiu Zhuang, and Chia-Yen Lee. Deep fake image detection based on pairwise learning. *Journal on Applied Sciences*, 10(1), 2020. **1, 2**
- [25] Xuefeng Hu, Zhihan Zhang, Zhenye Jiang, Syomantak Chaudhuri, Zhenheng Yang, and Ram Nevatia. Span: Spatial pyramid attention network for image manipulation localization. In *ECCV*, pages 312–328, Cham, 2020. Springer International Publishing. **1, 2**
- [26] Yihao Huang, Felix Juefei-Xu, Qing Guo, Yang Liu, and Geguang Pu. Fakelocator: Robust localization of gan-based face manipulations. *IEEE Trans. Inform. Forensics and Security*, 17:2657–2672, 2022. **1, 2, 6**
- [27] Minyoung Huh, Andrew Liu, Andrew Owens, and Alexei A. Efros. Fighting fake news: Image splice detection via learned self-consistency. In *ECCV*, September 2018. **1, 2, 3, 6, 7**
- [28] Phillip Isola, Jun-Yan Zhu, Tinghui Zhou, and Alexei A. Efros. Image-to-image translation with conditional adversarial networks. In *2017 IEEE Conference on Computer Vision and Pattern Recognition (CVPR)*, pages 5967–5976, 2017. **1**

- [29] Liming Jiang, Ren Li, Wayne Wu, Chen Qian, and Chen Change Loy. Deepforensics-1.0: A large-scale dataset for real-world face forgery detection. In *CVPR*, June 2020. 1, 2, 6
- [30] Tero Karras, Miika Aittala, Samuli Laine, Erik Härkönen, Janne Hellsten, Jaakko Lehtinen, and Timo Aila. Alias-free generative adversarial networks. In M. Ranzato, A. Beygelzimer, Y. Dauphin, P.S. Liang, and J. Wortman Vaughan, editors, *NeurIPS*, volume 34, pages 852–863. Curran Associates, Inc., 2021. 1
- [31] Tero Karras, Samuli Laine, and Timo Aila. A style-based generator architecture for generative adversarial networks. In *CVPR*, June 2019. 1
- [32] Tero Karras, Samuli Laine, Miika Aittala, Janne Hellsten, Jaakko Lehtinen, and Timo Aila. Analyzing and improving the image quality of stylegan. In *CVPR*, June 2020. 1
- [33] Diederik Kingma, Tim Salimans, Ben Poole, and Jonathan Ho. Variational diffusion models. In M. Ranzato, A. Beygelzimer, Y. Dauphin, P.S. Liang, and J. Wortman Vaughan, editors, *NeurIPS*, volume 34, pages 21696–21707. Curran Associates, Inc., 2021. 1
- [34] Matthias Kirchner. Fast and reliable resampling detection by spectral analysis of fixed linear predictor residue. In *Proceedings of the 10th ACM workshop on Multimedia and security*, pages 11–20, 2008. 2
- [35] Matthias Kirchner and Jessica Fridrich. On detection of median filtering in digital images. In Nasir D. Memon, Jana Dittmann, Adnan M. Alattar, and Edward J. Delp III, editors, *Media Forensics and Security II*, volume 7541, page 754110. International Society for Optics and Photonics, SPIE, 2010. 2, 7
- [36] Zhen Li, Cheng-Ze Lu, Jianhua Qin, Chun-Le Guo, and Ming-Ming Cheng. Towards an end-to-end framework for flow-guided video inpainting. In *CVPR*, pages 17562–17571, June 2022. 5, 13
- [37] Yuchen Luo, Yong Zhang, Junchi Yan, and Wei Liu. Generalizing face forgery detection with high-frequency features. In *CVPR*, pages 16317–16326, June 2021. 1, 2, 6
- [38] Francesco Marra, Diego Gagnaniello, Davide Cozzolino, and Luisa Verdoliva. Detection of gan-generated fake images over social networks. In *IEEE Conf. Multimedia Inform. Processing and Retrieval*, pages 384–389, 2018. 2
- [39] Francesco Marra, Diego Gagnaniello, Luisa Verdoliva, and Giovanni Poggi. A full-image full-resolution end-to-end-trainable cnn framework for image forgery detection. *IEEE Access*, 8:133488–133502, 2020. 1, 2
- [40] Falko Matern, Christian Riess, and Marc Stamminger. Depth map fingerprinting and splicing detection. In *ICASSP*, pages 2782–2786, 2020. 1, 2
- [41] Owen Mayer, Belhassen Bayar, and Matthew C. Stamm. Learning unified deep-features for multiple forensic tasks. In *ACM Workshop on Information Hiding and Multimedia Security, IHMMSec '18*, New York, NY, USA, 2018. Association for Computing Machinery. 3
- [42] Owen Mayer and Matthew C. Stamm. Learned forensic source similarity for unknown camera models. In *ICASSP*, pages 2012–2016, 2018. 3
- [43] Owen Mayer and Matthew C. Stamm. Exposing fake images with forensic similarity graphs. *IEEE Journal of Selected Topics in Signal Processing*, 14(5):1049–1064, 2020. 1, 2, 3, 6, 7
- [44] Owen Mayer and Matthew C. Stamm. Forensic similarity for digital images. *IEEE Trans. Inform. Forensics and Security*, 15:1331–1346, 2020. 3
- [45] Trisha Mittal, Ritwik Sinha, Viswanathan Swaminathan, John Collomosse, and Dinesh Manocha. Video manipulations beyond faces: A dataset with human-machine analysis. *arXiv preprint arXiv:2207.13064*, 2022. 1, 6, 7, 12
- [46] Trisha Mittal, Ritwik Sinha, Viswanathan Swaminathan, John Collomosse, and Dinesh Manocha. Video manipulations beyond faces: A dataset with human-machine analysis. *arXiv preprint arXiv:2207.13064*, 2022. 5, 6
- [47] Alex Nichol, Prafulla Dhariwal, Aditya Ramesh, Pranav Shyam, Pamela Mishkin, Bob McGrew, Ilya Sutskever, and Mark Chen. Glide: Towards photorealistic image generation and editing with text-guided diffusion models. *arXiv preprint arXiv:2112.10741*, 2021. 1
- [48] Cecilia Pasquini and Rainer Böhme. Information-theoretic bounds for the forensic detection of downsampled signals. *IEEE Transactions on Information Forensics and Security*, 14(7):1928–1943, 2018. 2, 3
- [49] Tomas Pevny and Jessica Fridrich. Detection of double-compression in jpeg images for applications in steganography. *IEEE Trans. Inform. Forensics and Security*, 3(2):247–258, 2008. 2
- [50] Jordi Pont-Tuset, Federico Perazzi, Sergi Caelles, Pablo Arbeláez, Alex Sorkine-Hornung, and Luc Van Gool. The 2017 davis challenge on video object segmentation. *arXiv preprint arXiv:1704.00675*, 2017. 5, 13
- [51] A.C. Popescu and H. Farid. Exposing digital forgeries by detecting traces of resampling. *IEEE Trans. Signal Processing*, 53(2):758–767, 2005. 2
- [52] A.C. Popescu and H. Farid. Exposing digital forgeries by detecting traces of resampling. *IEEE Transactions on Signal Processing*, 53(2):758–767, 2005. 7
- [53] Alin C. Popescu and Hany Farid. Statistical tools for digital forensics. In Jessica Fridrich, editor, *International Workshop on Information Hiding*, pages 128–147, Berlin, Heidelberg, 2005. Springer Berlin Heidelberg. 2
- [54] Aditya Ramesh, Prafulla Dhariwal, Alex Nichol, Casey Chu, and Mark Chen. Hierarchical text-conditional image generation with clip latents, 2022. 1
- [55] Iain E. Richardson. *The H.264 Advanced Video Compression Standard*. Wiley Publishing, 2nd edition, 2010. 7
- [56] Robin Rombach, Andreas Blattmann, Dominik Lorenz, Patrick Esser, and Björn Ommer. High-resolution image synthesis with latent diffusion models. In *CVPR*, pages 10684–10695, June 2022. 1
- [57] Robin Rombach, Andreas Blattmann, Dominik Lorenz, Patrick Esser, and Björn Ommer. High-resolution image synthesis with latent diffusion models. In *Proceedings of the IEEE/CVF Conference on Computer Vision and Pattern Recognition (CVPR)*, pages 10684–10695, June 2022. 1

- [58] Alexander Schlögl, Tobias Kupek, and Rainer Böhme. Forensicability of deep neural network inference pipelines. In *ICASSP 2021-2021 IEEE International Conference on Acoustics, Speech and Signal Processing (ICASSP)*, pages 2515–2519. IEEE, 2021. 2, 3
- [59] Matthew Stamm and K.J. Ray Liu. Blind forensics of contrast enhancement in digital images. In *IEEE Intl. Conf. Image Processing*, pages 3112–3115, 2008. 2
- [60] Supasorn Suwajanakorn, Steven M. Seitz, and Ira Kemelmacher-Shlizerman. Synthesizing obama: Learning lip sync from audio. *ACM Trans. Graph.*, 36(4), jul 2017. 1
- [61] Suramya Tomar. Converting video formats with ffmpeg. *Linux Journal*, 2006(146):10, 2006. 5
- [62] Sheng-Yu Wang, Oliver Wang, Andrew Owens, Richard Zhang, and Alexei A. Efros. Detecting photoshopped faces by scripting photoshop. In *ICCV*, October 2019. 1, 2
- [63] Sheng-Yu Wang, Oliver Wang, Richard Zhang, Andrew Owens, and Alexei A. Efros. Cnn-generated images are surprisingly easy to spot... for now. In *CVPR*, June 2020. 2
- [64] Ting-Chun Wang, Ming-Yu Liu, Jun-Yan Zhu, Andrew Tao, Jan Kautz, and Bryan Catanzaro. High-resolution image synthesis and semantic manipulation with conditional gans. In *CVPR*, pages 8798–8807, 2018. 1
- [65] Xintao Wang, Yu Li, Honglun Zhang, and Ying Shan. Towards real-world blind face restoration with generative facial prior. In *Proceedings of the IEEE/CVF Conference on Computer Vision and Pattern Recognition (CVPR)*, pages 9168–9178, June 2021. 1
- [66] Yue Wu, Wael AbdAlmageed, and Premkumar Natarajan. Mantra-net: Manipulation tracing network for detection and localization of image forgeries with anomalous features. In *CVPR*, pages 9535–9544, 2019. 1, 2, 6, 7
- [67] Chao Yang, Huizhou Li, Fangting Lin, Bin Jiang, and Hao Zhao. Constrained r-cnn: A general image manipulation detection model. In *ICME*, pages 1–6, 2020. 1, 2
- [68] Xin Yang, Yuezun Li, and Siwei Lyu. Exposing deep fakes using inconsistent head poses. In *ICASSP*, pages 8261–8265, 2019. 1, 2
- [69] Luo Yu, Yujin Zhang, Hua Han, Lijun Zhang, and Fei Wu. Robust median filtering forensics by cnn-based multiple residuals learning. *IEEE Access*, 7:120594–120602, 2019. 1, 2
- [70] Ning Yu, Larry S. Davis, and Mario Fritz. Attributing fake images to gans: Learning and analyzing gan fingerprints. In *ICCV*, October 2019. 2
- [71] Houssam Zenati, Manon Romain, Chuan-Sheng Foo, Bruno Lecouat, and Vijay Chandrasekhar. Adversarially learned anomaly detection. In *IEEE Intl. Conf. Data Mining*, pages 727–736, 2018. 2
- [72] Ru Zhang, Feng Zhu, Jianyi Liu, and Gongshen Liu. Depth-wise separable convolutions and multi-level pooling for an efficient spatial cnn-based steganalysis. *IEEE Trans. Inform. Forensics and Security*, 15:1138–1150, 2020. 1, 2
- [73] Hanqing Zhao, Wenbo Zhou, Dongdong Chen, Tianyi Wei, Weiming Zhang, and Nenghai Yu. Multi-attentional deepfake detection. In *CVPR*, pages 2185–2194, June 2021. 1, 2, 6
- [74] Peng Zhou, Xintong Han, Vlad I. Morariu, and Larry S. Davis. Learning rich features for image manipulation detection. In *CVPR*, June 2018. 1, 2
- [75] Yipin Zhou, Zhaowen Wang, Chen Fang, Trung Bui, and Tamara L. Berg. Dance dance generation: Motion transfer for internet videos. In *ICCVW*, pages 1208–1216, 2019. 1

Appendix

A. Code

In order to provide transparency and reproducibility towards the results presented in this paper, we have included VideoFACT’s network code and example code for training/evaluating our model. These files are stored in a zip file called `code.zip`. The whole code for this project and trained weights for the network will be publicly available under our research group’s gitlab page upon the publication of this work [this link is temporary hidden to preserve our anonymity under the double blind review process].

B. Dataset Creation

B.1. Set A: Standard Video Manipulations Datasets

In this section, we presents more details regarding the creation of the Standard Video Manipulations datasets used in this paper, specifically, those used for training and validation of our network - VCMS, VPVM, VPIM.

In order to generate samples for each of these datasets, we first needed to make binary masks which specify the to-be-manipulated regions in video frames/images. To facilitate this process, we created a library of 10 basic shapes: rectangle, circle, ellipse, triangle, pentagon, heptagon, 5-pointed star, 8-pointed star, 12-pointed star, and 18-pointed star. Since we wanted to avoid our network overfitting to any particular shapes, we further constructed complex compound shapes by overlapping up-to three basic shapes in a random manner. After the compound shapes for each mask were finalized, it was randomly resized, randomly rotated, and translated to a random location inside the mask’s boundary (1080×1920). We note that masks with the manipulated area greater than 75% of the total area were rejected and regenerated using the same procedure.

With the binary masks ready, we then applied either splicing operations (copying content from a source video/image and pasting it into a destination video/image), or in-place editing operation (manipulating each frames of a video or image). With regards to in-place editing operations, we manipulated the regions specified by the mask with at least one of the following operations: changing brightness, contrast, saturation, and hue, adding random Gaussian blur, random motion blur, random box blur, and random Gaussian noise. We used the open-source differentiable computer vision library Kornia to perform these edits. The parameters used for the perceptually visible datasets (VPVM) and the perceptually invisible datasets (VPIM) are listed in the Table B1.

Finally, we re-encoded the authentic video frames of each authentic video into the set of authentic videos and the manipulated videos frames of each manipulated video into the set of manipulated videos. All videos were re-encoded as

Visible?	Manip. Type	Manip. Parameters	Manip. Prob.
Yes	Brightness	range=[0.8, 1.6]	1.0
	Contrast	range=[0.7, 1.3]	1.0
	Saturation	range=[0.8, 1.1]	1.0
	Hue	range=[-0.2, 0.2]	1.0
	Gaussian Blur	kernel.size=(5,5), sigma=(2,2)	0.7
	Motion Blur	kernel.size=(5,5), angle=[-25, 25], direction=[-1, 1], resample='BICUBIC'	0.7
	Box Blur	kernel.size=(5,5)	0.7
No	Gaussian Noise	std=0.05	1.0
	Brightness	range=[0.95, 1.05]	0.9
	Contrast	range=[0.95, 1.05]	0.9
	Saturation	range=[0.95, 1.05]	0.9
	Gaussian Blur	kernel.size=(3,3), sigma=(1.2,1.2)	0.7
	Motion Blur	kernel.size=(3,3), angle=[-20, 20], direction=[-1, 1], resample='BICUBIC'	0.7
	Box Blur	kernel.size=(3,3)	0.7
	Gaussian Noise	std=0.006	0.9

Table B1. This table lists the different parameters used to manipulate a victim video frame or victim image so that the manipulated area is either perceptually visible or invisible. These parameters are passed into different augmentation modules available in the open-source differentiable computer vision library Kornia.

H.264 videos using FFmpeg with the constant rate factor of 23 and the frame rate of 30 FPS.

Note that, in addition to the three video datasets made using the process described above, we also created three Standard Image Manipulation datasets in the exact same procedure. This resulted in three auxiliary image datasets: ICMS, IPVM and IPIM.

A summary of all datasets are listed in Table B2, B3, B4

B.2. Set B: In-the-Wild Manipulated Datasets

In addition to evaluating on our Standard Video Manipulation datasets, we tested our proposed network and other network on three In-the-Wild Manipulated datasets: VideoSham, Inpainted Video and Deepfake Video.

The **VideoSham** dataset used in this paper was a subset of the one published by Adobe Research [45]. We excluded videos with audio track or temporal manipulations and videos with resolution less than 1080p. Hence, the remaining manipulated videos were attacked by 1) adding objects/subjects, 2) removing objects/subjects, 3) background/object’s color change and 4) adding/removing text. Since the masks indicating the manipulation regions were missing from the original dataset, we created them by first dividing both the manipulated frame and the original frame into small, non-overlapping blocks (16×16), then

computing the average luminance-value absolute difference across 3 channels (R, G, B) between each original and manipulated block. After we produced a scalar value for every block, we normalized these values so that they were between 0 and 1 and thresholded them so that they became binarized. We then projected the binary value of each blocks to all the pixel locations belong to that block in order to create a binarized pixel-level masks indicating the manipulated region.

The **Inpainted Video** dataset was generated by replacing objects in a scene with their background. In order to leverage existing state-of-the-art video inpainting algorithms like E2FGVI-HQ, we needed videos in which some to-be-removed objects were segmented across multiple frames. Therefore, we chose the Densely Annotated Video Segmentation (DAVIS) dataset [50] for this purpose because it contains both the original videos and the ground-truth segmentation masks for foreground objects in those videos. Inputting a video and its masks into the network code provided publicly by the authors of E2FGVI-HQ [36], and using the recommended settings, we generated videos in which the segmented objects were inpainted over. Since the resolution of the output videos were 540p, we resized them up to 1080p so that they could be analyzed by our proposed network. We applied this process over all 90 videos in the DAVIS dataset to get 90 inpainted videos, which we used for evaluation.

The **Deepfake Video** dataset was made by creating deepfaked videos of celebrity interview videos downloaded from YouTube. These downloaded videos were first trimmed down to maximum of 30 seconds, where the only primary subject on the scene was a human body with its face clearly visible. We then chose one source-destination video pair from our set of downloaded videos to perform face swapping. Note that faces of the similar skin tone and gender were more likely to result in better quality deepfakes. We then extracted all faces from the frames of the source and destination video. These faces were then aligned and learned by a deep neural network architecture from DeepFaceLab [16]. After we trained the deepfake network, we used it to perform face-swapping for each uncompressed frame. Finally, these frames were compressed into an H.264 video using FFmpeg with the constant rate factor of 23 and the frame rate of 30 FPS. Using this procedure, we generated 10 deepfaked videos, in which we took out continuous 30 frames chunk from each video to make the Deepfake Video dataset.

C. Run Time Analysis

In this section, we provide a preliminary run time analysis of our network and other competing networks: FSG, EXIFnet, Noiseprint, ManTra-Net and MVSS-Net. These run time benchmarks are gathered using unoptimized code, taken directly from other authors' publicly available code repositories. Therefore, these results do not represent the

Dataset	Original		Manipulated	
	# of Frames	# of Videos	# of Frames	# of Videos
VCMS	48000	1600	48000	1600
VPVM	48000	1600	48000	1600
VPIM	48000	1600	48000	1600
ICMS	48000	N/A	48000	N/A
IPVM	48000	N/A	48000	N/A
IPIM	48000	N/A	48000	N/A

Table B2. Summary of our training datasets.

Dataset	Original		Manipulated	
	# of Frames	# of Videos	# of Frames	# of Videos
VCMS	7800	260	7800	260
VPVM	7800	260	7800	260
VPIM	7800	260	7800	260
ICMS	7800	N/A	7800	N/A
IPVM	7800	N/A	7800	N/A
IPIM	7800	N/A	7800	N/A

Table B3. Summary of our validation datasets.

Group	Dataset	Original		Manipulated	
		# of Frames	# of Videos	# of Frames	# of Videos
A	VCMS	4200	140	4200	140
	VPVM	4200	140	4200	140
	VPIM	4200	140	4200	140
B	VideoSham	7897	32	12746	64
	Inpainted Video	9312	90	9312	90
	Deepfake Video	300	10	300	10

Table B4. Summary of the datasets used for evaluating the performance of our network and others.

Network	Average Analysis Frame Rate (FPS)
Proposed	30.80
FSG	1.82
EXIFnet	0.04
Noiseprint	0.57
ManTra-Net	0.40
MVSS-Net	26.06

Table C1. This table shows the average run time (number of samples per second) of our network and competing networks.

best potential run time of these algorithms. They only show what one may experience the run time of each algorithm by directly using other authors' publicly available code. We performed this analysis on a machine with an NVIDIA RTX 3090 GPU, a 12th Gen Intel i9-12900KF CPU (24 cores at 5.200 Ghz), 64 GB of DDR4 (2800Mhz) RAM, running Ubuntu 22.04.1 with Kernel version 5.15.0-52-generic. We ran 1000 samples individually, each of size $1080 \times 1920 \times 3$, through each network, recorded the total run time, then reported the average run time as frames per second (FPS).

From Table C1, we see that our network achieves the highest FPS, or fastest run time when compared to competing networks. Additionally, with a FPS of over 30, our network is capable of real-time video processing, which can be very useful in practical scenarios.

D. Additional Examples From Each Dataset and Their Localization Results

In this section, we show additional representative examples from each dataset along with their localization results from our proposed network and other competing networks: FSG, EXIFnet, Noiseprint, ManTra-Net and MVSS-Net.

A brief discussion and interpretation of the results for

each dataset is provided in each figure’s caption. Results for the VCMS dataset are presented in Figure D1, results for the VPVM dataset are presented in Figure D2, results for the VPIM dataset are presented in Figure D3, results for the Deepfake Video dataset are presented in Figure D4, results for the Inpainted Video dataset are presented in Figure D5 and results for the VideoSham dataset are presented in Figure D6.

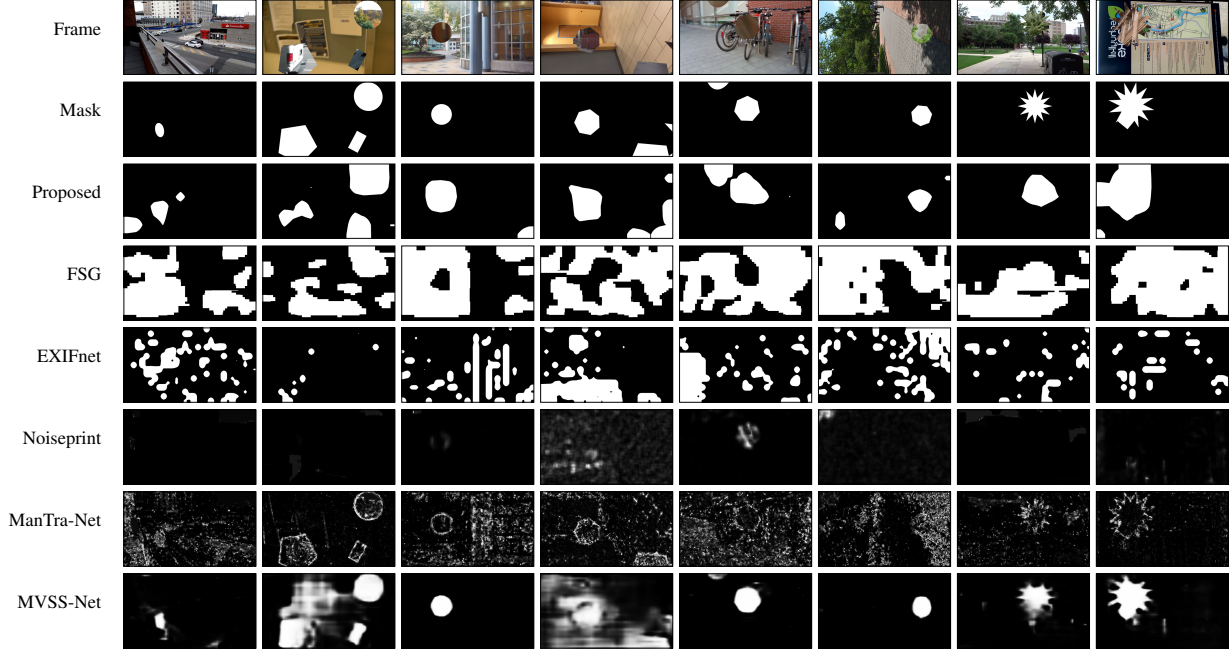


Figure D1. This figure shows the localization results of different networks on the VCMS dataset. Our proposed network’s localization results are good, with some minor false alarms on column 1, 3, 6 and 9. We note that, our predicted masks are blobs, which means a large source of our pixel-level localization error comes from the fact that we cannot predict shapes with sharp, concave edges. By contrast, networks, which leverage edge information, like ManTra-Net and MVSS-Net were able to produce masks with sharp edges. Hence, MVSS-Net were comparable to our network in terms of localization performance. On the other hand, FSG, EXIFnet and Noiseprint did not seem like they could make reasonable predictions about the manipulation region.

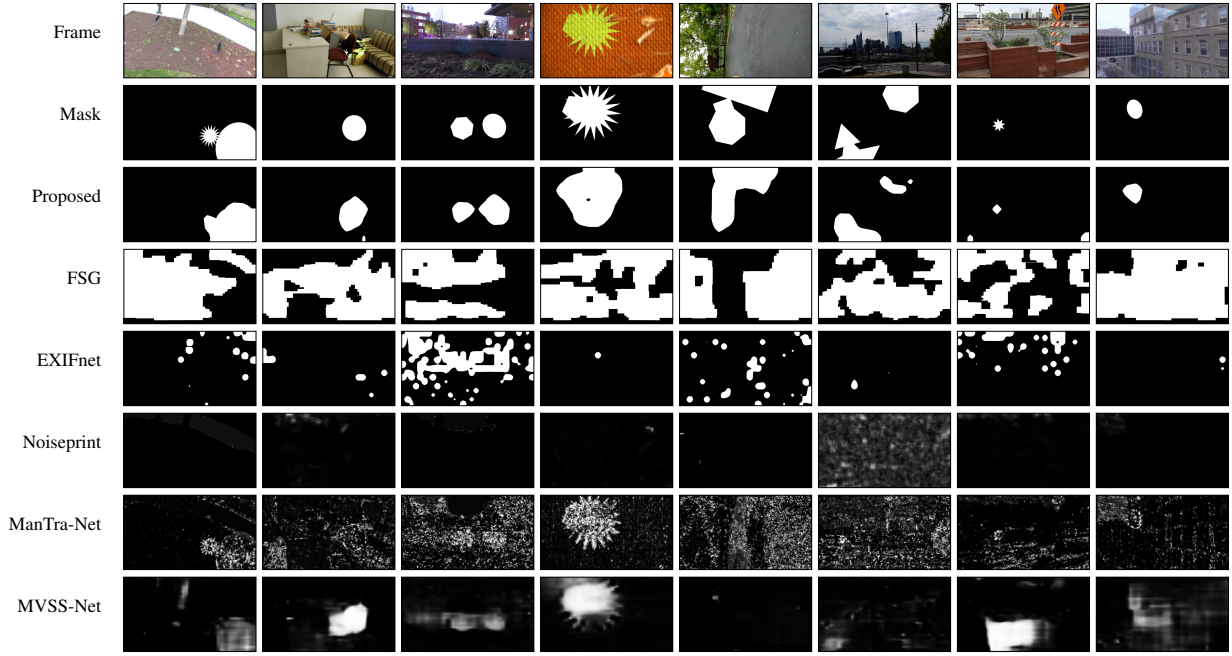


Figure D2. This figure shows the localization results of different networks on the VPVM dataset. Our proposed network’s localization results are good, with some minor false alarms on column 2 and 7. Again, our predicted masks are blobs, which means a large source of our error comes from the fact that we cannot predict shapes with sharp, concave edges. Nonetheless, contrast to results on VCMS, strong competitors like MVSS-Net and Mantra-Net could not identify the manipulated region unless it was extremely visible (e.g column 1, 2, 3 and 4). Other examples contained manipulations which resulted in perceptually visible edges but it seemed like competing algorithms false alarmed on regions which had distinct textures versus the rest of the frame, such as they sky (column 3, 6, 8), the colored bricks (column 7), and the building (column 8).

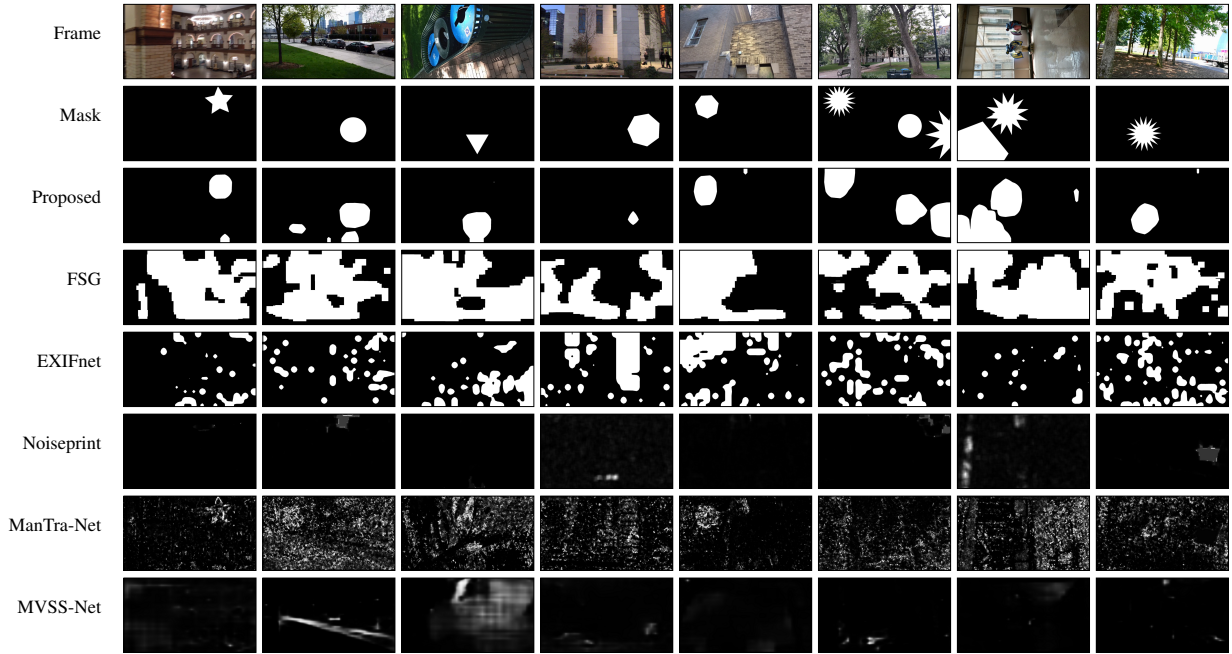


Figure D3. This figure shows the localization results of different networks on the VPIM dataset. Our proposed network’s localization results are strong, with some minor false alarms on column 1, 2 and mis-detections on column 4. Differs from VCMS and VPVM, in this dataset, the manipulations’ strengths were so low that they are largely perceptually invisible. Hence, in contrast to our network, other competing networks failed to provide any meaningful predictions of the manipulated region.



Figure D4. This figure shows the localization results of different networks on the Deepfake Video dataset. Our proposed network’s localization results are reasonable, with minor false alarms on column 1, 2, 3, 7 and mis-detections on column 4. Our network was able to largely identify the deepfaked faces in each of these example. However, for scenes similar to column 4, in which both the manipulated region and its surrounding regions had poor lighting condition, our network’s performance seemed to be lower. Notably on column 7, although only the face was manipulated, we were able to detect the watermarked logo on the top right of the frame as well. This prediction is reasonable since the watermark was added in post-processing, hence, it could be considered an additional manipulation. Since other competing networks seemed to be identifying the entire body or the surrounding regions with distinct textures to be manipulated, they did not provide good localization performance in this dataset.

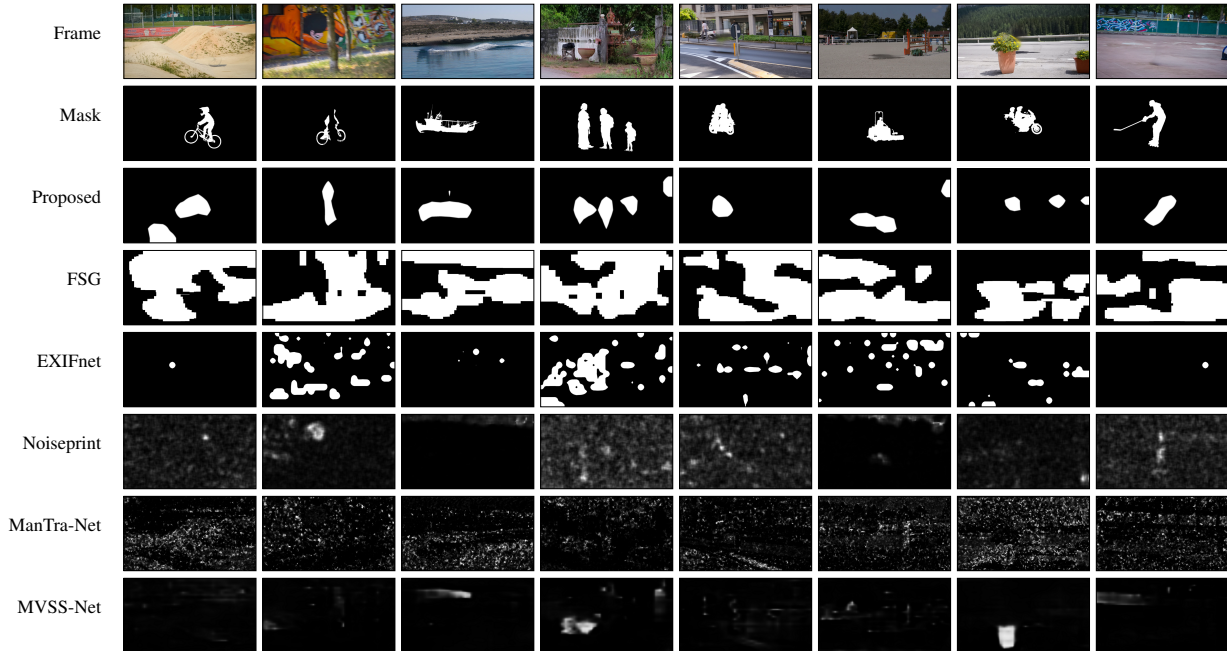


Figure D5. This figure shows the localization results of different networks on the Inpainted Video dataset. Our proposed network’s localization results are reasonable, with false alarms on column 1, 4, 6, 7 and mis-detections on column 7. Our network were able to largely identify the regions where the segmented objects were removed. On column 7, although our network misdetected the removed motorbike on this frame, we were able to occasionally catch it in other frames of the video. Generally, when the video was stable, without a lot of moving objects, we were able to reliably detect the manipulated regions. However, if the camera moved around too quickly, the frame was blurred, which made our network less likely to provide accurate predictions. While our network generalized well over this dataset, other competing networks failed to identify any manipulations in these videos. We suspected that since objects were removed, there existed no edge information for these networks to rely on, and the residual information might be too different for them to behave properly.



Figure D6. This figure shows the localization results of different networks on the VideoSham dataset. Our proposed network's localization results are reasonable, with minor false alarms on column 1, 2, 3 and mis-detections on column 3, 4, 5. Our network were able to largely identify the manipulated regions in each of these example. However, on scenes like column 4 where the manipulated region was too small, it was not possible for our network and other competing networks to detect. Our network also missed two added books in the back on columns 3, likely because their sizes were small. Additionally, on column 5, where the color of the wall on the right was changed from blue to red, our network failed to identify the entire manipulated region. Other than these errors, our network produced reasonable localization results, while other competing methods largely failed to identify any manipulations.